Heliyon 10 (2024) e27883

Contents lists available at ScienceDirect

Heliyon

journal homepage: www.cell.com/heliyon

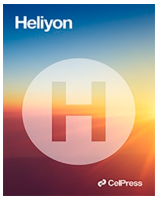

Research article

Method for *in situ* polypyrrole coating, and the example of its use for functionalization of polyurethane anisotropic electrospun mats

Leona Mahelová [a], Petr Slobodian [a,b], Karolína Kocourková [b], Antonín Minařík [a,b], Robert Moučka [a], Miroslava Trchová [c], Martina Martínková [a], Kateřina Skopalová [a], Zdenka Víchová [a], Věra Kašpárková [a,d], Petr Humpolíček [a,d,*]

[a] *Centre of Polymer Systems, University Institute, Tomas Bata University in Zlín, Trida T. Bati 5678, 76001, Zlin, Czech Republic*
[b] *Department of Physics and Materials Engineering, Faculty of Technology, Tomas Bata University in Zlin, Vavreckova 5669, 76001, Zlin, Czech Republic*
[c] *Central Laboratories, Laboratory of Molecular Spectroscopy, University of Chemistry and Technology Prague, Technicka 5, 166 28 Prague 6, Czech Republic*
[d] *Department of Fat, Surfactant and Cosmetics Technology, Faculty of Technology, Tomas Bata University in Zlin, Vavreckova 5669, 76001, Zlin, Czech Republic*

ARTICLE INFO

Keywords:
Coating
Conductivity
Image analysis
Anisotropy
Stem cells

ABSTRACT

The *in situ* coating of polymer substrate with polypyrrole, described herein with detailed know-how, represents a novel technique of surface functionalization. The choice of oxidizing agent and the polymerization time both affect the properties of the thin polypyrrole layer. The specific conductivity, free surface energy, thickness, topography, and FTIR spectra of polypyrrole layer were determined. The conductive coatings were further used to functionalize both isotropic and anisotropic electrospun polyurethane nanofibrous mats to show their applicability and study the bioactive effect of both the anisotropy and conductivity together. The morphology of composites was studied by means of atomic force microscopy and scanning electron microscopy. A complex cytocompatibility study was performed, including determining cytotoxicity by optical and fluorescence microscopy, the advanced qualification of cell morphology by cell-image analysis, and a study of stem cell behavior. The results clearly showed the significant impact of substrate modification on cells, especially on fibroblasts while the embryonic stem cells were less affected. This study shows not only the effective way to prepare a thin conducting layer based on polypyrrole but also demonstrates its importance for the fabrication of smart biomaterials.

1. Introduction

The successful application of polymers in tissue engineering is conditioned by an understanding of their interaction with cells, which is influenced by a number of material properties. The material's good **electrical conductivity** offers notable advantages in many tissues, especially electrosensitive ones (e.g., cardiac or neural tissue). Conductive scaffolds mimic the native conductivity of tissues, thereby promoting cell-substrate interactions, cell-cell communication, and cell signaling, leading to improved tissue integration and functionality. Also, conductive scaffolds can provide a platform for controlled electrical stimulation, which creates an

* Corresponding author. Tomas Bata University in Zlín, Trida T. Bati 5678, 76001, Zlin, Czech Republic.
E-mail address: humpolicek@utb.cz (P. Humpolíček).

https://doi.org/10.1016/j.heliyon.2024.e27883
Received 25 September 2023; Received in revised form 4 March 2024; Accepted 7 March 2024
Available online 13 March 2024

environment that guides cell behavior; for example, enhances cell growth and migration, expedites nerve regeneration, or promotes cardiomyogenesis [1–4]. In this context, electrically conductive polymers (CPs) are at the center of attention, mainly thanks to their intrinsically combined electron- and ion-based conductivity.

Among CPs, polypyrrole (PPy) is a promising representative due to its high conductivity and stability. The study by Wang et al. (2004) confirmed that PPy extracts do not induce acute or subacute toxicity, hemolysis, allergenicity, or mutagenesis *in vivo* [5]. On the other hand, Hsu et al. (2008) identified the limits of PPy cytocompatibility when PPy is in contact with various tissues [6]. *In vitro* studies then showed that there are differences between the cytotoxicity and embryotoxicity of PPy salt and PPy base [7] and that low molecular products present in PPy base can induce neurogenesis in embryonic stem cells [8]. In addition, an improvement in cell/PPy interactions can be obtained by adjusting many factors, such as the method of synthesis (chemical or electrochemical) and the various conditions of synthesis, the used oxidation agents and dopant ions, and even the rinsing procedure [9].

Regarding oxidation agents, iron(III) chloride ($FeCl_3$) [9–13], ammonium persulfate (APS) [13,14], sodium persulfate [15] hydrogen peroxide [16], cupric chloride [17], phosphomolybdic acid [18], and many others can be used for the PPy synthesis. In the here presented study, the former two oxidants in the list were employed and compared. The choice of oxidant has a considerable effect on the resulting cytocompatibility and other key properties, such as the electrical conductivity [19]. Previous studies utilized PPy in the form of powders [20–23], co-polymers [24–26], or colloidal dispersions [27–29], though, only a few studies are concerned with PPy *in situ* coating [30–32] and even less are put in the connection with its cytocompatibility [33].

The **surface properties** of a biomaterial play a critical role in cell/material interaction. According to Ravichandran et al. (2010), the major limitation on the cytocompatibility of PPy (and conductive polymers in general) is its hydrophobicity, which decreases the successful entrapment of proteins to the surface [34]. Nevertheless, this disadvantage can be overcome by doping with various anionic dopants [20] or by the coating of PPy with extracellular matrix components [35]. These allow the initial adhesion and growth of cells, which subsequently produce their own extracellular matrix and thus colonize the surfaces more easily.

For the best results with respect to cytocompatibility, the **topography** of biomaterials should be modified at both the micro-scale and nano-scale depending on the type of cultured cells [36]. The topographical treatment of materials is an economically effective way of improving the biological activity of any biomaterial surface. The principle is that a surface structure determines the availability of suitable binding sites for adhesive proteins, thereby affecting their surface distribution. As a result, biomaterials with topographic modifications acquire capabilities that were originally reserved only for growth factors [37]. This is related to the fact that most types of cells can sense the orientation, texture, and physical properties of biomaterials [38].

Moreover, a biomaterial's **iso/anisotropy** plays a crucial role. This is related to the fact that the extracellular matrix is often anisotropic *in vivo* [39]. Many studies have aimed to simulate the *in vivo* anisotropic structure of the myocardium through a series of topographical features, because cardiomyocytes establish their native *in vivo* phenotype – aligned actin fibers, parallel sarcomeric arrangements, and nuclear elongation [40] and the contractile properties of cardiac tissues are directly related to cellular orientation and elongation. In fact, not only cardiomyocytes but the majority of cell types cultured on grooved profiles elongate and align themselves along the major axis of the topographic anisotropic surface features, such as grooves [41]. In response to the anisotropic topography, uniaxially oriented nanofibers have also been reported to induce morphological changes in many cell types, including cytoskeletal rearrangements, nuclear elongation, and even axon extrusion from neuronal stem cells [42,43].

Iso/anisotropy can thus be considered another cell-instructive material property, especially when discussing stem cell behavior. However, CPs, e.g. PPy, cannot form solid materials themselves and thus their topography and anisotropy cannot be controlled. The preparation of composites, therefore, seems to be the most effective solution to this problem. Previously, cryogels of various polymers with either PPy or polyaniline were prepared [44,45] but the adjustability of their anisotropy was limited. A more effective approach is to prepare a composite combining an anisotropic substrate with the surface functionalization with CPs.

In the present study, electrospun polyurethane (PU) mats were combined with PPy to prepare composites (**PUPPy**) with controllable anisotropy, topography, and conductivity. This study contributes to the current knowledge of substrate coating with PPy and its impact on cytocompatibility.

As the main novelty, we present a method that makes the process of coating a substrate with PPy as simple, fast and versatile as possible, so it is applicable to any substrate; such as the nanofibrous nonwoven mats reported here. Previously reported PPy coating methods are certainly functional, but require the involvement of electricity in the process [46], or specific solvents [47] or stabilizers [48], furthermore they may be limited by the long polymerization time [33] and, last but not least, the low temperature during the reaction process [47–50]. In comparison to these, here presented PPy coating is synthesized chemically *in situ* in aqueous solution at room temperature in seconds without the use of any stabilizers or modifiers, resulting in a uniform thin layer with high conductivity. Therefore, the method allows for the use of PPy coating in a common practice or big manufacturing facility. A drawback of this method may be its speed. Since the reaction occurs quickly, we emphasize the importance of controlling the polymerization time of PPy, as exceeding the time has a negative effect on the topography and leads to the disruption of the PPy coating.

Another strength of our study is the quantitative and qualitative cell-image analysis, which graphically illustrates the impact of the anisotropic topography of the nanofibrous substrate, the electrical conductivity of the PPy coatings, and their combinations on cell morphology. On the basis of previously described knowledge, we hypothesized that coating an anisotropic substrate with conducting PPy will lead to the preparation of a cell-instructive composite. The study presents a complex cytocompatibility experiment employing electrospun nonwoven nanofiber PU mats both in their pristine and modified forms. Three types of modifications were tested:

1. An uniaxial orientation of fibers in the PU mats to achieve anisotropy;
2. Coating the oriented PU mats with PPy to enhance electro-conductivity;
3. Coating the PUPPy composite with gelatin and albumin to increase cytocompatibility.

The effects of these modifications on the behavior of a mouse fibroblast cell line and a mouse embryonic stem cell line were observed.

2. Materials and methods

2.1. Electrospinning, purification, and orientation of nanofibrous nonwoven PU mats

Desmopan 385 S (Covestro AG, Germany) was dissolved in a 3:1 solvent mixture of dimethylformamide (Brenntag, Poland) and methylisobutylketon (Penta Chemicals, Czech Republic) to a concentration of 12.5 %. The final solution had a viscosity of 1.3 Pa s and a conductivity of 31.5 mS/cm due to the addition of sodium chloride (Penta Chemicals, Czech Republic). Then, the solution was loaded into syringes connected to 32 jets of the electrospinning device Nanospider (Elmarco, Czech Republic). The solution was extruded into a high-voltage electric field (75 kV). A planar collector with a backing film drawn at a speed of 0.1 m/min was located 19 cm from the jets. The final product had 4 deposited layers with a basis weight of 9.01 g/m^2.

To remove impurities and unbound residues, such as solvents and salts, from the manufacture, the electrospun PU mats measuring (15 × 15) cm^2 were immersed in 500 mL of ultrapure water and shaken for 7 d, while the water was changed every 48 h, and then dried for 1 h at 50 °C.

Next, these isotropic PU mats with randomly oriented fibres were taped to the microscope cover glass. To obtain anisotropic PU mats with aligned fibres, the PU mats were manually stretched 1 cm over a heat source at 150 °C and attached in the stretched state with tape to the microscope cover glass without any delay. In both cases, overlaps were cut off to obtain a uniform area of (22 × 22) mm^2.

2.2. Synthesis of PPy coatings

PPy *in situ* synthesis was used to coat the surfaces of various substrates. First, cell culture dishes were coated with PPy and the properties of PPy coatings such as topography, thickness, specific conductivity, surface free energy, and basic cytocompatibility were analyzed on these coated dishes. Secondly, indium tin oxide (ITO) glass was used as a support suitable for FTIR spectroscopy analysis of deposited PPy thin layers. Finally, the electrospun PU fibrous mats were coated with PPy to create PUPPy composites. The structure and biocompatibility of the latter materials were then studied in detail.

The PPy *in situ* polymerization was conducted using pyrrole (Sigma-Aldrich, USA) as a monomer and APS (Sigma-Aldrich, USA) or $FeCl_3$ (IPL, Czech Republic) as an oxidation agent. Solutions of the monomer (0.2 M) and the oxidation agent (0.25 M) in ultrapure water were prepared and allowed to stand for about 1 h at room temperature conditioned at 20 °C before being pipetted into cell culture dishes (empty or containing ITO glass supports or PU mats) in a ratio of 1:1. The polymerization reaction was carried out for 15 s (t_1), 30 s (t_2), or 60 s (t_3) at room temperature conditioned at 20 °C. To terminate the PPy coating formation, the excess reaction mixture was discarded and the surfaces covered with PPy coatings were immediately and thoroughly rinsed with 0.2 M hydrochloric acid (Penta Chemicals, Czech Republic), which had two roles here: It washed out the residual unreacted substances and at the same time doped the PPy coatings. Then, the resulting substrates with PPy coatings were rinsed with methanol (Penta Chemicals, Czech Republic) and allowed to dry overnight at room temperature conditioned at 20 °C.

The variation in polymerization time is presented here to demonstrate its significant influence on the topography of the final PPy coatings. Besides that, all subsequent syntheses and analyses were performed on samples prepared with the same polymerization time: (t_1) = 15 s, which was chosen as the most appropriate because it resulted in the most uniform surface. Furthermore, PUPPy composites were formed by oxidizing PPy with $FeCl_3$ only, which was selected for its superior cytocompatibility.

2.3. Characterization of physicochemical properties

Atomic force microscopy (AFM): The surface topographies of PPy coatings synthesized on cell culture dishes using various oxidizing agents and reaction times were measured by means of a Dimension ICON atomic force microscope (Bruker Corporation, USA). Measurements were performed at a scan rate of 0.5 Hz with a resolution of (512 × 512) pixels in tapping mode in an air atmosphere at room temperature (22 °C, 50 % RH). A silicone-nitride probe with a resonant frequency of 70 ± 25 kHz and a spring constant of 0.4 N/m (ScanAsyst-Air, Bruker) was used.

The morphology of PUPPy composites was studied using an NTEGRA Prima (NT-MDT) atomic force microscope in tapping mode in air in an atmosphere at room temperature (22 °C, 50 % RH). An NSG01 (TipsNano) silicon probe of force constant 1.45–15.1 N/m was used. The sample area was scanned at a rate of 0.4 Hz in (512 × 512) pixel format.

Thickness measurements of PPy coatings on cell culture dishes surfaces were scanned using AFM. A silicone rubber mask was attached to the cell culture dishes before and during the PPy coating process. After polymerization was terminated, the silicone mask was removed to prepare clean edges for the thin PPy layers. AFM characterization was performed using a Dimension ICON in ScanAsyst mode using ScanAsyst-Air silicon nitride probe with a spring constant of 0.4 N/m (Bruker Corporation, USA). The measurements were performed under laboratory conditions (temperature and atmosphere). The scanning rate was 0.5 Hz.

Images were processed using Gwyddion – Free SPM data analysis software, version 2.55 (D. Nečas, P. Klapetek, Czech Metrology Institute, Czech Republic). The images were edited using Data Levelling and Background Subtraction – functions Plane level and Polynomial Background. Profile sections were made in the middle of the measured area. The parameters R_a (the arithmetic average surface roughness value) and R_z (average peak-to-valley depth profile parameter) were obtained from 3 profile sections.

Specific conductivity: The electric conductivity of PPy coatings deposited on cell celture dishes was determined at room temperature by the four-point van der Pauw method. A Keithley 6517B electrometer, a Keithley 2410 source meter, and a Keithley 7002 switch (USA) were used.

Surface free energy: Measurements of contact angles on PPy coatings in cell celture dishes were carried out by a Theta Optical Tensiometer (Biolin Scientific, Finland). For all PPy coatings, demineralized water, ethylene glycol, and diiodomethane (Sigma-Aldrich, USA) were used as test liquids. The sessile static droplets with a volume of 10 μL were used and contact angles were recorded after (10 ± 2) s at room temperature. The measurement was repeated ten times for each sample. The surface free energy was determined using the "acid-base" method.

FTIR spectroscopy: The spectra of thin PPy coatings deposited on ITO support were obtained using a Thermo Scientific Nicolet iN10 Infrared Microscope with a Thermo Scentific Omnic Picta user interface equipped with a liquid nitrogen cooled MCT-A detector (mercury cadmium telluride) in reflection micro-spectroscopic mode. The spectra were measured in the spectral range 4000–650 cm^{-1} with the resolution 4 cm^{-1}, 64 scans and Happ-Genzel apodization. The aperture of the microscope was set to (150 × 150) μm^2.

Scanning electron microscopy (SEM): Surface images of PUPPy composites were obtained by a Phenom Pro SEM, (Phenom-world BV). For SEM observation, the PUPPy composites were cut into pieces (4 × 4) mm^2, fixed on stubs by conductive tape, and coated with gold and palladium. Samples were observed at an acceleration voltage of 10 kV in backscattered electron mode with a magnification of 4000 × . Images were processed in ImageJ software, version 1.53k (W. Rasband, National Institutes of Health, United States).

2.4. Preparation for and conditions of biological testing

Sterilization: The sterilization of all PPy coatings and PUPPy composites was accomplished by UV radiation for 30 min of each side.

Coating with bio-substances: To enhance the cytocompatibility of PPy coatings and PUPPy composites, solutions of bovine serum albumin (Sigma-Aldrich, USA) (40 mg/mL) and bovine gelatin (Sigma-Aldrich, USA) (0.1 %) in ultrapure water were applied to their surface. Three types of protein coatings were created on PPy coatings on cell culture dishes: 1) 1 mL of albumin solution only (Alb), 2) 1 mL of gelatin solution only (Gel), or 3) 0.5 mL of albumin solution and 0.5 mL of gelatin solution together (Alb/Gel). The last one was also used for coating PUPPy composites. The proteins from the solutions were allowed to adhere to the surfaces for 20 min. Then, the solutions with residual proteins were aspirated and surfaces were allowed to dry at room temperature for at least another 20 min.

Used cell lines: To describe the cytocompatiblity of the composites comprehensively, two cell lines were utilized. First, the mouse fibroblast cell line NIH/3T3 (ECACC 93061524, England) was applied. As a basis for the culture medium for fibroblats, Dulbecco's modified eagle's medium (DMEM) (BioSera, France) and sodium hydrogen carbonate (Penta, Czech Republic) were used. Then, calf serum (BioSera, France) (to the amount of 10 % of the total volume of the medium) and the antibiotics Penicillin/Streptomycin (BioSera, France) at a concentration of 100 μg/mL (to the amount of 1 % of the total volume of the medium with the serum together) were added to the DMEM. The second utilized cell line was the R1 mouse embryonic stem cell line [51]. For the cultivation for embryonic stem cells in an undifferentiated state, a culture medium based on DMEM (Gibco™, USA) was used. To the DMEM, the following supplements were added: fetal calf serum (BioSera, France) (to the amount of 16.5 % of the total volume of the medium), the antibiotics Penicillin/Streptomycin (BioSera, France) at a concentration of 100 μg/mL (to the amount of 1 % of the total volume of the medium with the serum together), 100 mM of non-essential amino acids (Gibco™, USA), 0.05 mM β-mercaptoethanol (Sigma-Aldrich, USA), and leukemia inhibitory factor (Chemicon, USA) at a concentration of 5 ng/mL.

Cell cultivation: Cells were cultivated in a biological incubator HERAcell 150i (Thermo Scientific, USA) with a controlled atmosphere of 5 % CO_2, temperature 37 °C, and constant relative humidity. Fibroblasts or embryonic stem cells at a concentration of 1 × 10^5 cells/mL of complete culture medium were seeded onto the surface of the PU mats, PUPPy composites, and references. As references, cell culture dishes were used for fibroblasts; however, for embryonic stem cells, cell culture dishes were gelatinized with 0.1 % porcine gelatin (Sigma-Aldrich, USA) in water. When cells had adhered to the surface (after 2 h), the aliquot part of the medium was added to achieve a volume of 2 mL. The samples with cells were then put in the incubator for 4 d with medium restitution every 2 d.

2.5. Evaluation of biological testing

Optical microscopy: In addition to regular visual checks of the cells, a phase contrast optical microscope (Olympus IX51, Japan) supplemented with a digital camera (Olympus E−450, Japan) was employed to obtain cell proliferation results from coated and seeded cell culture dishes. An optical microscope generally enables the quick and easy observation of living cells; however, the possibility of using it here was limited by the opacity of PU. Therefore, the PU mats and PUPPy composites were analyzed by fluorescence microscopy.

Fluorescence microscopy: Fluorescence microscopy was used for the further determination of cell morphology. Cells grown on the surfaces were rinsed with phosphate-buffered saline (BioSera, France), fixed with 2 mL of 4 % formaldehyde (Penta Chemicals, Czech Republic) in ultrapure water, and then permeabilized by 2 mL of 0.5 % Triton X 100 (Sigma-Aldrich, USA) in phosphate-buffered saline. Finally, the cells were stained with two fluorescent dyes: 1) ActinRed 555 or ActinGreen 488 (Life Technologies, USA) (1 drop/mL), which binds to the proteins in cytoskeletons, and 2) Hoechst 33258 (Sigma-Aldrich, USA) (20 μL/mL), which penetrates the nuclei where it binds to the DNA. The stained cells were observed by an Olympus IX 81 phase-contrast inverted fluorescence microscope (Olympus, Japan) with a Leica DFC480 camera (Leica Microsystems, Japan).

Quantification using CellProfiler software: Since all PUPPy composites had a unified surface area of (22 × 22) mm^2, it was

possible to perform a proper quantification of grown cells. As references, pre-cut bottoms of cell culture dishes with the same (22 × 22) mm^2 surface area were used. After 2 d of mouse fibroblast cultivation, the cells were fixed, stained, and photographed using the fluorescence microscope. Forty images of cell nuclei with 40 × magnification were manually acquired from the surface of each observed sample for further quatification. Five images of cytoskeletons and five images of cell nuclei with 100 × magnification were acquired from the surface of each observed sample for further morphology qualification. Image analysis was then performed using the open-access CellProfiler software 4.0.7 [52]. For the identification of stained nuclei and cytosceletons, the images were converted to grayscale, and any white regions caused by structural inequalities were excluded.

3. Results and discussion

3.1. Synthesis and characterization of PPy coatings

As commonly known and understood, the chemical synthesis is facile and relativelly quick procedure for producing CPs. The rate of chemical reaction can be, however, modified by several variables, such as the type and concentration of the oxidation agent, presence of dopants, change of temperature and reaction time [53]. The last factor is crucial, especially in the process of PPy coating synthesis. To create a uniform PPy layer, stopping the polymerization reaction at the right time is essential. Otherwise, PPy aglomerates start to grow as time progresses and break free from the surface, and eventually a poorly adhering powder is created instead of a thin PPy coating.

Topography: The PPy coatings prepared with different oxidation agents and reaction times on cell culture dishes were investigated by AFM. The obtained AFM visualization (Fig. 1) shows PPy particles within the thin coating layer that grow in size as the chemical reaction progresses. Coatings prepared at longer reaction times are difficult to observe by AFM, because the movement of detached particles causes defects in the pictures. This phenomenon was significantly worse in PPy coatings prepared using APS. The reason lies in the considerably higher reaction rate of the polymerization initiated by APS.

The fact that the topography of PPy coatings depends on the reaction time is also supported by the roughness analysis, as shown in Table 1. The R_z parameter, which represents the height difference between the highest and the lowest points of the surface, increases gradually with the reaction time length. This dependence is valid for both PPy^{APS} and PPy^{FeCl3}. The average surface roughness parameter R_a is also the lowest for both PPy coatings prepared in the shortest time (t_1) of 15 s. Also when comparing the measured values, the surface roughness of PPy^{APS} is significantly higher than that of PPy^{FeCl3}, which corresponds to the discussion of the AFM images in Fig. 1.

Based on these results, it is clear that the most uniform coating is obtained by the shortest reaction time. Since this setting has the greatest potential for further studies, the following experiments and measurements were performed on PPy coatings synthesized with the reaction time $(t_1) = 15$ s only. These PPy coatings on cell culture dishes were further studied to better understand their physiological properties and to distinguish between the effects of two various oxidizing agents.

Thickness: The PPy coatings were prepared with different oxidation agents on cell culture dishes with an attached silicon mask used to create clean edges observable by AFM. As can be seen in Fig. 2, AFM profilometry indicated the PPy^{APS} and PPy^{FeCl3} coatings to have different thicknesses. The former, PPy^{APS} coating, has the thickness of approximately 50 nm, while the later, PPy^{FeCl3} coating, is about 30 nm thick.

Specific conductivity: Conductivity measurements on PPy coatings deposited on cell culture dishes prepared with various oxidation agents (reaction time (t_1) 15 s) were performed by the four-point van der Pauw method, which is a commonly used technique for measuring the resistivity and conductivity of thin film or sheet-like samples [54–56]. Results of this measurement are strongly

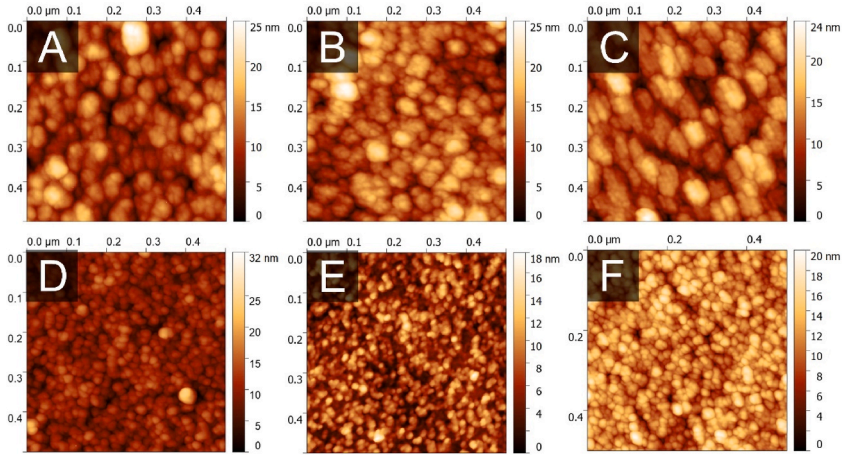

Fig. 1. AFM of PPy coatings on cell culture dishes (0.5 × 0.5) μm^2. PPy^{APS} (up A to C), PPy^{FeCl3} (down D to F). Reaction times: (t_1) 15 s (left column), (t_2) 30 s (middle column), (t_3) 60 s (right column).

Table 1
Roughness analysis of PPy^{APS} and PPy^{FeCl3} coatings prepared in (t_1) 15 s, (t_2) 30 s, and (t_3) 60 s. The errors represent standard deviations.

	(t_1) 15 s		(t_2) 30 s		(t_3) 60 s	
	R_a [nm]	R_z [nm]	R_a [nm]	R_z [nm]	R_a [nm]	R_z [nm]
PPy^{APS}	2.26 ±0.04	12.8 ±1.4	2.6 ±0.3	14.0 ±1.7	2.52 ±0.17	16.5 ±0.4
PPy^{FeCl3}	1.79 ±0.13	9.4 ±0.7	1.92 ±0.11	10.9 ±0.6	1.87 ±0.04	11.7 ±0.3

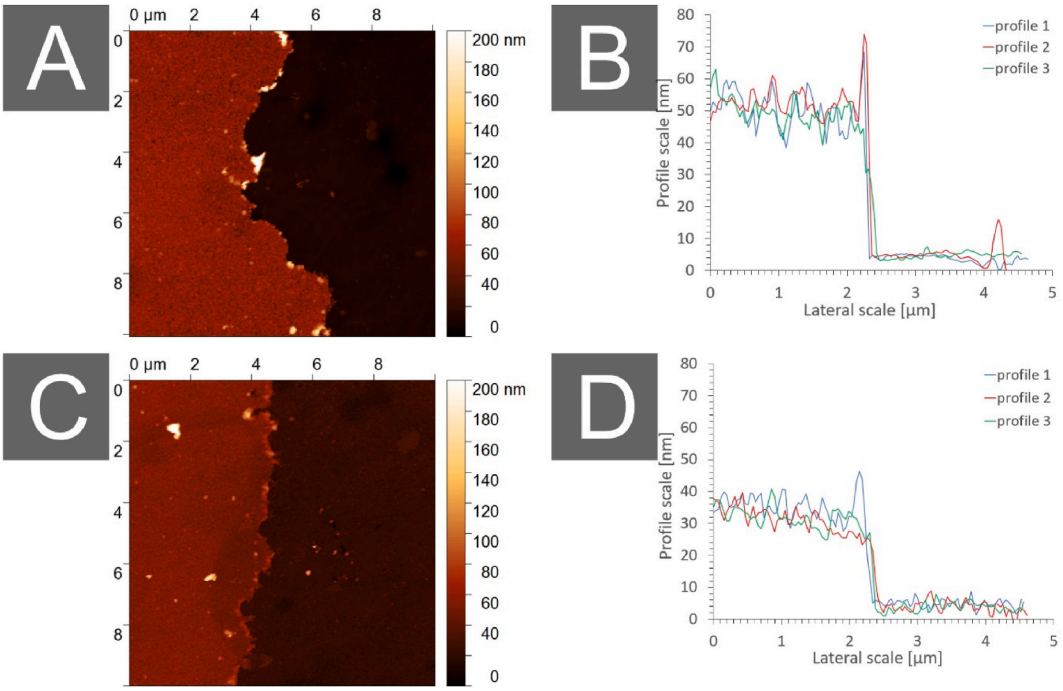

Fig. 2. AFM profilometry of the edges of PPy coatings on cell culture dishes (10 × 10) µm². PPy^{APS} (A,B), PPy^{FeCl3} (C,D). Reaction time: (t_1) 15 s.

dependent on the coating thickness, so it was necessary to calculate the actual measured thicknesses from Fig. 2 to obtain comparable data and that highlighted some differences. According to the results, PPy^{APS} demonstrated higher specific conductivity, concretely 85.03 ± 0.05 S/cm, in comparison to PPy^{FeCl3}, which had a specific conductivity of 67.22 ± 0.01 S/cm.

In general, the conductivity of PPy strongly depends on many factors (discussed in the introduction), mainly the synthesis method, conditions, and especially doping. Therefore, thin PPy layers prepared through chemical synthesis of monomer and oxidant exhibit conductivity in a wide range from zero or very low conductivity (~10^{-10} S/cm) to nearly 2 × 10^3 S/cm [47,53,54,57–59].

Surface free energy: The contact angles measured on PPy coatings on cell culture dishes prepared with various oxidation agents for the reaction time (t_1) 15 s are shown in Table 2. On both PPy^{APS} and PPy^{FeCl3}, water contact angles were slightly above the Berg limit of $\sigma = 65°$ [60,61]; thus, both may be considered mildly hydrophobic. The results further indicate very close values for the total surface energy (γ^{TOT}) of all samples: 43.9 ± 2.0 mJ/m² for PPy^{FeCl3}, and 44.5 ± 0.9 mJ/m² for PPy^{APS}. However, the dispersive Lifshitz-van der Waals component (γ^{LW}) and the polar acid-base component (γ^{AB}) showed variations of around 6 mJ/m². In both cases, the electron-acceptor parameter (γ^{+}) was almost negligible. On the other hand, the electron-donor parameter (γ^{-}) was twice as high for PPy^{FeCl3} – in numerical values, 16.0 ± 2.5 mJ/m².

Table 2
Contact angles and surface free energy of PPy^{APS} and PPy^{FeCl3} coatings on cell culture dishes prepared in (t_1) 15 s. The errors represent standard deviations.

	Contact angles σ = [deg]			Surface energy components γ = [mJ/m²]				
	water	ethylene glycol	diiodo-methane	γ^{TOT}	γ^{LW}	γ^{AB}	γ^{+}	γ^{-}
PPy^{APS}	70±8	30.3±1.7	44.1±0.7	44.5±0.9	37.5±0.4	7.0±0.8	1.6±0.8	8±4
PPy^{FeCl3}	67±3	41±3	32.0±1.4	44±2	43.4±0.4	0.5±1.7	0.00±0.06	16±3

FTIR spectra: FTIR spectroscopy was performed to confirm the successful polymerization of PPy. Since cell culture dishes are made of polystyrene which is unsuitable for FTIR spectroscopy, ITO glass was used as a substrate for the PPy coating. As shown in Fig. 3, the FTIR spectra of PPy obtained in reflection mode on an ITO substrate prepared *in situ* using APS or $FeCl_3$ oxidant for the reaction time (t_1) 15 s are weak, but practically identical to the spectrum of granular PPy dispersed in KBr used as a reference. They exhibit bands situated at 1543 cm^{-1} (C–C stretching vibrations in the pyrrole ring), at 1454 cm^{-1} (C–N stretching vibrations in the ring), the broad band with a maximum at about 1305 cm^{-1} (C–H or C–N in-plane deformation modes), and a maximum at 1166 cm^{-1} (breathing vibrations of the pyrrole rings). The band at 1042 cm^{-1} corresponds to C–H and N–H in-plane deformation vibrations, while the peaks with maxima at about 894 and 786 cm^{-1} correspond to the C–H out-of-plane deformation vibrations of the ring [62].

3.2. Cytocompatibility optimization of PPy coatings

Although many studies report PPy to be a cytocompatible material [5,63], this study shows its limitations. The cell response to polymer surface may be negatively affected by its hydrophobicity [34] and low values of the electron-donor component of free surface energy [64]. These features of PPy coatings may be controlled through different factors, such as the used oxidizing agents and dopants, the conditions of synthesis, and post-synthesis fate. In this study, the resulting water contact angles for both PPy^{APS} and PPy^{FeCl3} (Table 2) were decreased almost down to the Berg limit of $\sigma = 65°$ [60,61]. As shown in Fig. 4 B and F, NIH/3T3 mouse fibroblasts tended to die on these PPy surfaces. Slightly better cytocompatibility was observed on PPy^{FeCl3} which has somewhat higher electron-donor component (Table 2); however, the results were still not sufficient for successful cell adhesion and proliferation.

According to Satriano et al. (2003), the presence of serum proteins reduces the impact of the electron-donor component and the cell response is rather dependent on the total value of the surface free energy [64]. Furthermore, Azioune et al. (2002) report that electrochemically synthesized PPy films (with values of surface free energy components close to ours) demonstrate hydrophobic interactions with human serum albumin and that such PPy films strongly adsorb proteins [20].

Therefore, the PPy coatings prepared on cell culture dishes with the reaction time (t_1) 15 s were further biofunctionalized by the adhesion of selected bio-substances Alb and Gel as these change the biological activity of the treated surface [35,65]. As the results in Fig. 4 show, the presence of Alb or Gel on the PPy-coating increased its cytocompatibility; however, the combination of both Alb/Gel together led to the most significant cytocompatibility improvement. These positive results, which were likely achieved due to functional carboxyl and amino groups of proteins and peptides, comply with studies by Wu et al. (2020) [66] and Van Vlierberghe et al. (2011) [67], which confirmed the biocompatibility and cell-interactive properties of albumin and gelatin.

3.3. Anisotropy of PUPPy composites

Further in this study, **PPy^{FeCl3}** and **Alb/Gel** were used to coat electrospun PU fibrous mats to prepare cytocompatible PUPPy composites with controlled conductivity and topography at the same time. Modification and control of topography can improve material bioactivity as it imitates natural cellular environment. In the case of nanofibrous scaffolds, the uniaxial orientation of fibers can be advantageous since the extracellular matrix of soft tissues are mostly anisotropic, except for, for example, the basal lamina. Nevertheless, attention should also be paid to mechanical anisotropy, which increases with fiber alignment [68].

The orientation of fibers in native electrospun PU mats is random, which makes the substrate isotropic. To obtain the uniaxial orientation of fibers, the PU mats were stretched by hand over a 150 °C heat source. After cooling in the stretched state, the PU mats retain their fibre orientation even after the stretching force is removed. The SEM and AFM images of the PUPPy composites presented in Fig. 1 show the effectiveness of this modification. As can be seen, the isotropic PUPPy composites (Fig. 5 A, C, E) consist of randomly oriented fibers. Topographic measurements of their cross-sections showed that irregularities of up to 3 μm in size were formed on the

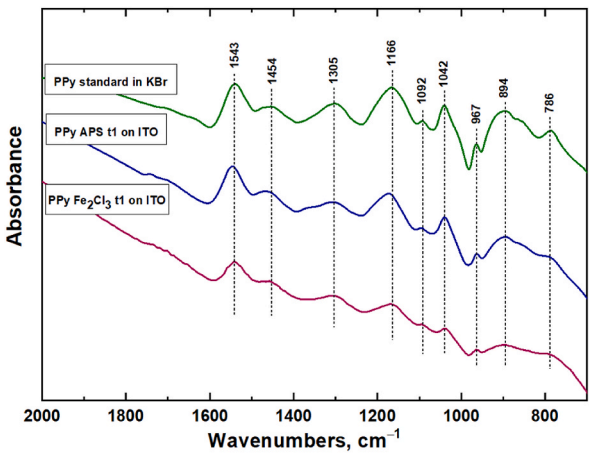

Fig. 3. FTIR spectra of PPy obtained in reflection mode on ITO support prepared *in situ* using APS or $FeCl_3$ oxidant for the reaction times (t_1) 15 s. The spectrum of granular PPy dispersed in KBr is included for comparison.

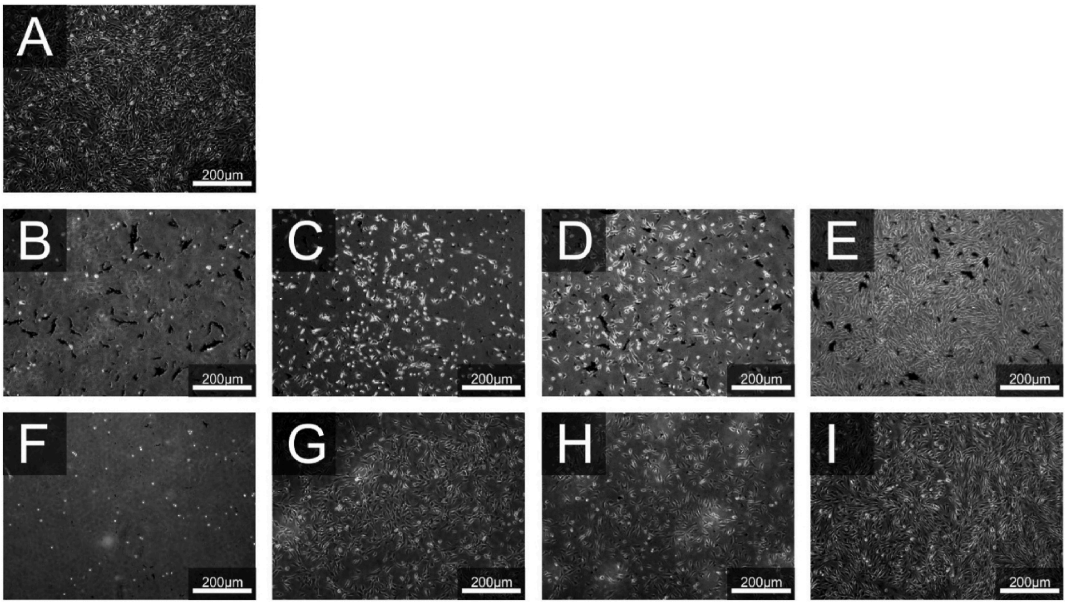

Fig. 4. Optical microscopy images of NIH/3T3 mouse fibroblasts cultivated on PPy-based coatings on cell culture dishes: (**A**) Reference, (**B**) PPy^{APS}, (**C**) PPy^{APS} with Alb, (**D**) PPy^{APS} with Gel, (**E**) PPy^{APS} with Alb/Gel, (**F**) PPy^{FeCl3}, (**G**) PPy^{FeCl3} with Alb, (**H**) PPy^{FeCl3} with Gel, (**I**) PPy^{FeCl3} with Alb/Gel. Reference cells were cultivated in cell culture dishes. All the images were captured after 72 h of cell culture at magnification 40 × .

surface, while the fiber diameter was approximately 0.5 μm. In contrast, fibers in the anisotropic PUPPy composites (Fig. 5 B, D, F) appear to be highly oriented, the heights of topographic features remaining similar. The surface roughness analysis also showed no significant differences between isotropic and anisotropic PUPPy. The roughness parameters of isotropic PUPPy were R_a = (0.38 ± 0.02) nm and R_z = (2.16 ± 0.09) nm, while anisotropic PUPPY had R_a = (0.31 ± 0.03) nm and R_z = (2.4 ± 0.3) nm. In general, although some fibers were torn after the manual stretching, the majority of the fibers lie in one direction. Therefore, this quick and easy way of aligning fibers may be considered successful.

3.4. Cytocompatibility of PUPPy composites

The impact of iso/anisotropic properties and conductivity on the morphology of NIH/3T3 mouse fibroblasts and R1 mouse embryonic stem cells was observed by means of fluorescence microscopy.

Fig. 6 shows how PPy coatings (with Alb/Gel) and fiber alignment affect the mouse fibroblast NIH/3T3 cell line. The effect of fiber orientation on the cytoskeleton is significant. Cells grown on isotropic PU mats (Fig. 6 B) primarily show a stellate-like morphology, similar to the shapes of fibroblasts cultivated as the reference in cell culture dishes (Fig. 6 A). In contrast, cells grown on anisotropic PU mats (Fig. 6 C) adopt distinctly prolonged shapes in the exact direction of the orientation of fibers. Further, many of these cells also possess elongated nuclei compared to the rounded cell nuclei on isotropic PU mats.

These results confirm the claim made by Yin et al. (2010) that cells respond to fiber orientation with cytoskeletal changes and the elongation of nuclei [43]. The explanation probably lies in contact guidance and cell-matrix interactions, whose amounts and distributions are influenced by the nanofiber alignment, which plays an important role in regulating cell functions, including proliferation and migration (distribution).

With respect to the conductive surface coating, it also significantly influences cell morphology, as can be seen, for example, in the case of isotropic PUPPy composites (Fig. 6 D). Cell cytoskeletons preferably assume rounded and lenticular shapes with a random direction because of the randomly oriented fibers in the substrate; the nuclei of these cells are classically rounded. The observed rounding of the fibroblast cytoskeletons may have been due to altered focal adhesion dynamics or cytoskeletal remodeling in response to the conductive coating of PPy. However, it should be noted that other factors, such as the change in the physical and mechanical properties of the PU substrate after coating with PPy and Alb/Gel, may also have an influence. The composition and distribution of the proteins bound to the substrate surface can affect the morphology of various cell lines [69]. The cultivation of fibroblasts on anisotropic PUPPy composites (Fig. 6 E) leads apparently to more spindle-shaped cytoskeletons; however, the surface coating prevents nuclei elongation; nevertheless, the orientation of cells is still according to the fiber orientation. In addition, it can be observed a reduction in protrusion formation in fibroblasts seeded on PUPPy composites. This may indicate a modulation of cell motility towards a more targeted and controlled behavior that is essential for processes in tissue regeneration and wound healing.

To determine the impact of the prepared PU mats and PUPPy composites on NIH/3T3 mouse fibroblast proliferation, a comparative quantitative assay was conducted. An analysis of 200 images was performed using CellProfiler software [52]. The results are shown in Fig. 7. As can be seen in the graph, the cells proliferated least on the isotropic PU mat (0.22), while on the anisotropic PU mat (0.87),

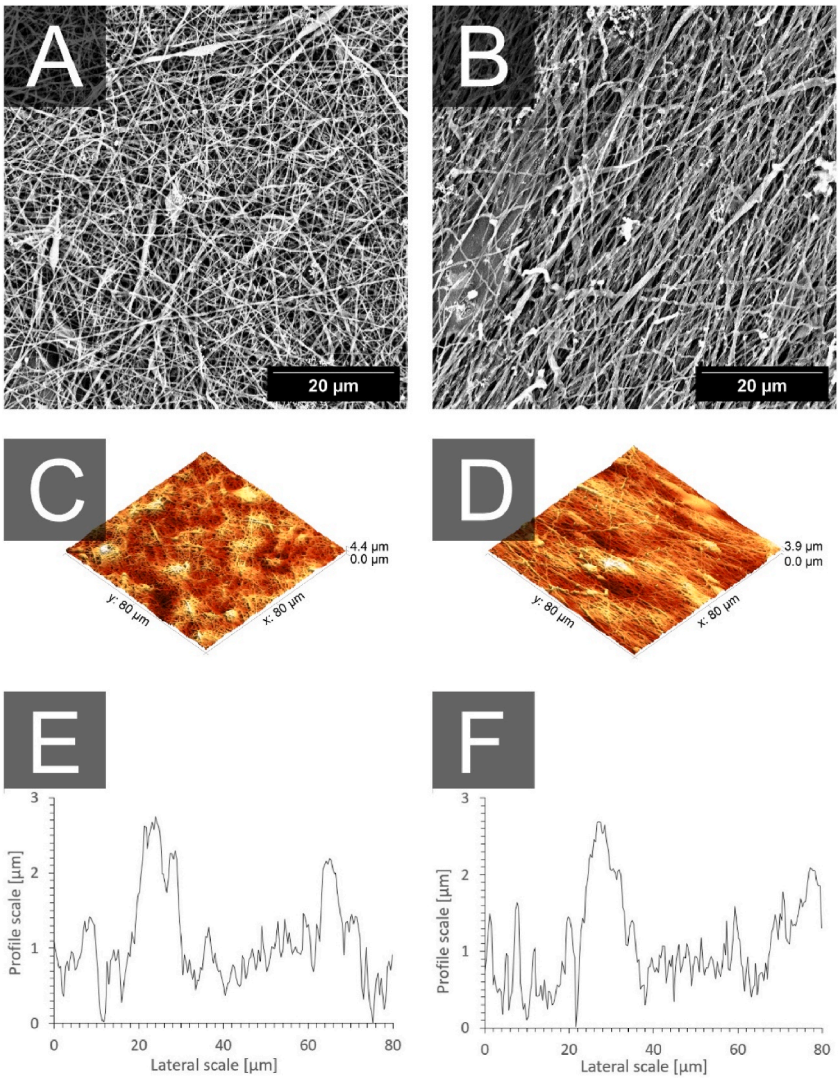

Fig. 5. Surface characterization of PUPPy composites: (**A, C, E**) Isotropic form with randomly oriented fibers; (**B, D, F**) Anisotropic form with uniaxially oriented fibers; (**A, B**) SEM images; (**C, D**) AFM images; (**E, F**) Profile sections.

the relative cell viability was comparable to the reference (1.00). It thus seems that the alignment of fibers itself has a significant impact on fibroblast well-being. On the other hand, the PPy^{FeCl3} coating with Alb/Gel used to create PUPPy composites removed this dependence, as cell viability was the same on both isotropic and anisotropic PUPPy composites (0.62). From this it can be concluded that the conductive PPy coating provides a uniform semi-favorable surface for fibroblast proliferation irrespective of the substrate underneath. This ensures a controlled and homogeneous cell spreading and attachment and thus the formation of a more stable cell network, similarly to the article by Tringides and Mooney (2024), where the formation of a uniform cell network was achieved with increased conductivity of their hydrogel scaffolds [70]. The results were verified using a one-way ANOVA with post-hoc Tukey's test, which showed whether the means of the measured values were statistically significantly different at the levels of significance $p \leq 0.05$ (*), $p \leq 0.01$ (**), or $p \leq 0.001$ (***).

In addition to the quantitative assay, a qualitative analysis of 50 images of NIH/3T3 mouse fibroblasts was also carried out using CellProfiler software [52]. Results in the form of four graphs are shown in Fig. 8, together with an explanatory scheme of crucial cell characteristics. First, each observed object (a cell or a nucleus) was translated into the best-fitting ellipse with the same second moments and statistical properties as the original area. The morphology of the cells, especially their elongation (Fig. 8 B), was then depicted by the length of the major and minor axes of the best-fitting ellipse and their comparison. The resulting median values of the measured cells clearly show that the fibroblasts grown on the anisotropic PU mat possessed the most prolonged shapes - the greatest lengths (major axes) and the thinnest widths (minor axes). In contrast, a comparatively rounded cell morphology was induced by PPy coatings, as may be observed for both the isotropic and anisotropic PUPPy composites.

The orientation of cells (Fig. 8 C) is displayed as an angle, written as θ in the explanatory scheme, between the x-axis and the major

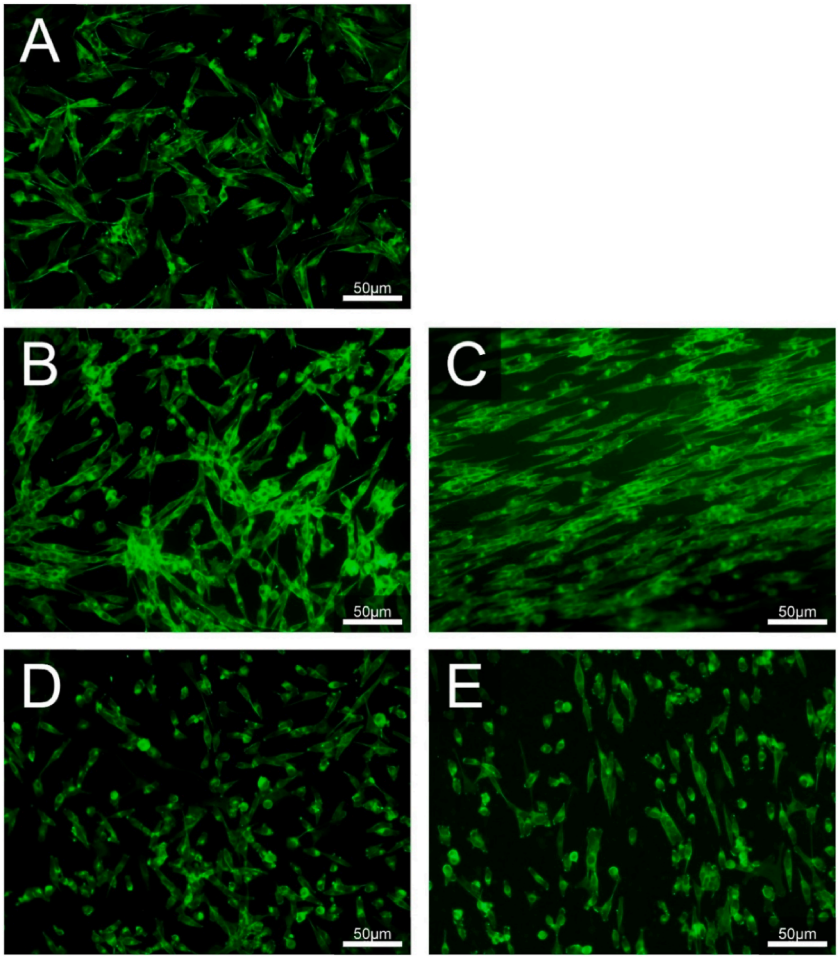

Fig. 6. Fluorescence microscopy images of NIH/3T3 mouse fibroblasts cultivated on: (**A**) Reference; (**B**) isotropic PU mat; (**C**) anisotropic PU mat; (**D**) isotropic PUPPy composite with Alb/Gel; (**E**) anisotropic PUPPy composite with Alb/Gel. Reference cells were cultivated in cell culture dishes. Green color: ActinGreen – actin. Magnification: 100 × . (For interpretation of the references to color in this figure legend, the reader is referred to the Web version of this article.)

axis of the best-fitting ellipse. For example, reference fibroblasts cultivated in cell culture dishes show random orientations, meaning randomly various angles from $-\pi/2$ to $+\pi/2$, which lead to a median close to 0 with a wide deviation. Very similar values were also obtained for cells grown on all other substrates except one – the anisotropic PU mat. Here, most cells were oriented uniaxially along the fiber direction, resulting in a given orientation and a very small standard deviation.

The morphology of cell nuclei (Fig. 8 E) was also analyzed. In the graph, the nucleus shape is described by an eccentricity defined as the ratio of the distance between the foci, written as F_1 and F_2 in the explanatory scheme, of the best-fitting ellipse and its major axis length. Values can vary from 0 (an ideal circle) to 1 (a line segment). As can be seen, the observed cells have relatively elongated nuclei, as is usual for fibroblasts – however, some more than others. Anisotropic PU mats established nuclei with higher eccentricity (0.73) than other observed substrates (around 0.63). These results suggest a correlation in the elongation of cell cytoskeleton and nuclus. The analysis of nuclei orientation (Fig. 8 F) was consistent with the orientation of cells (Fig. 8 C). This implies that the PPy coating prevented both the elongation and uniaxial orientation of fibroblasts and their nuclei.

All these outputs of the qualitative analysis of fibroblasts are in accordance with the morphological differences observed by fluorescence microscopy described in Fig. 6. The results were verified using one-way or two-way ANOVA tests with post-hoc Tukey's test, which showed whether the means of the measured values were statistically significantly different at the levels of significance $p \leq 0.05$ (*), $p \leq 0.01$ (**), or $p \leq 0.001$ (***).

Images of mouse embryonic stem cells cultivated on PU mats and PUPPy composites are shown in Fig. 9. No significant differences in cell behavior were found on any of the tested samples. Cells did not differ in proliferation, managed to survive in an undifferentiated state (in the presence of a medium containing leukemia inhibitory factor), and did not tend to grow apart on the surface at all; contrarywise, they clustered. Embryonic stem cells typically form dense clusters of various sizes and shapes when cultured in cell culture dishes (Fig. 9 A). The same behaviour of embryonic stem cells was observed on all tested substrates (Fig. 9 B – E). Clusters of

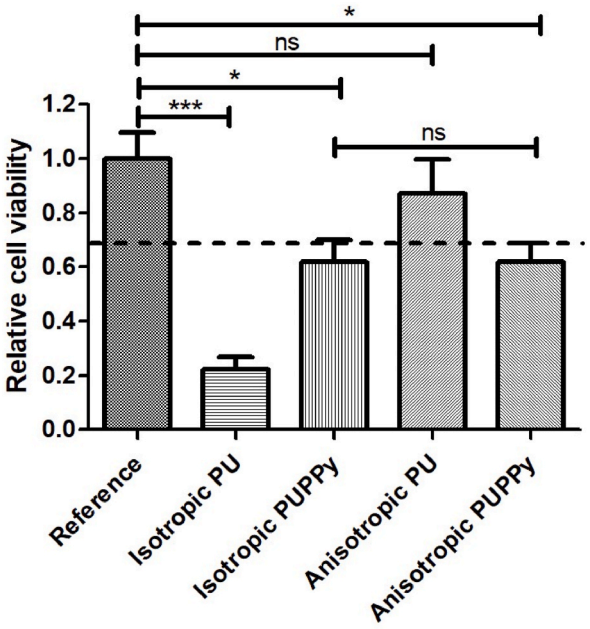

Fig. 7. Results of image analyses performed by CellProfiler software referring to the cytocompatibility of iso/anisotropic PU mats and PUPPy composites with the NIH/3T3 mouse fibroblast cell line. Reference cells were cultivated in cell culture dishes. Error bars show standard error of mean. One-way ANOVA with post-hoc Tukey's test: ns = $p > 0.05$, * = $p \leq 0.05$, *** = $p \leq 0.001$.

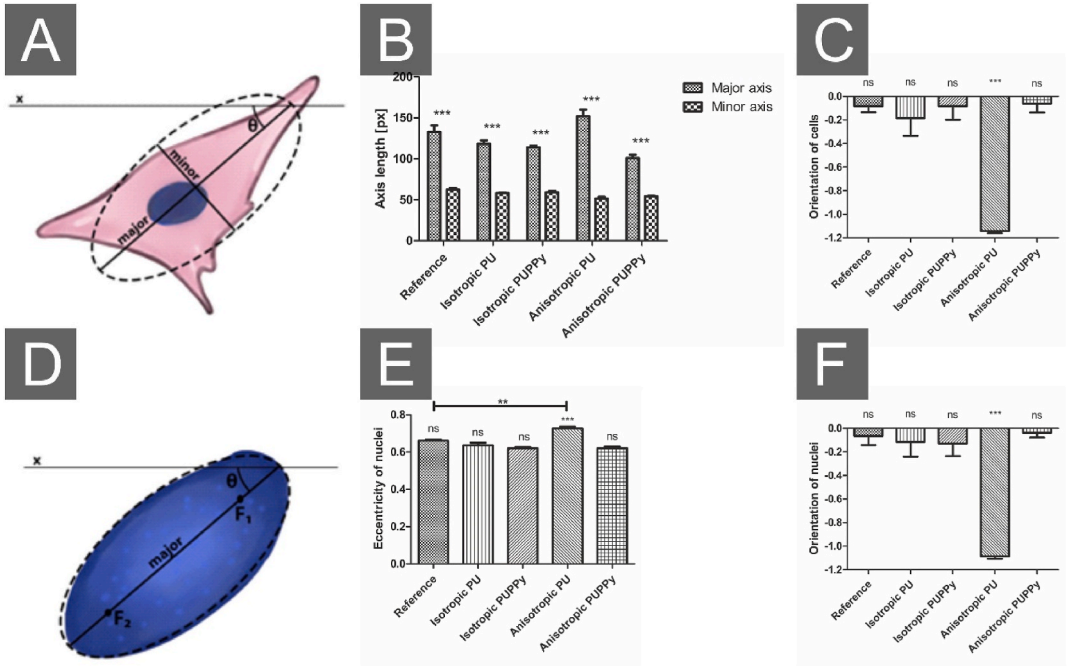

Fig. 8. Results of image analyses performed by CellProfiler software referring to NIH/3T3 mouse fibroblasts cultivated on iso/anisotropic PU mats and PUPPy composites. Explanatory schemes of calculated characteristics related to: (A) cells, (D) nuclei. Graphs: (B) morphology of cells, (C) orientation of cells, (E) eccentricity of nuclei, and (F) orientation of nuclei. Reference cells were cultivated in cell culture dishes. Error bars show standard error of mean. Two-way ANOVA for (B) and one-way ANOVA for (C, E, F) with post-hoc Tukey's test: ns = $p > 0.05$, ** = $p \leq 0.01$, *** = $p \leq 0.001$.

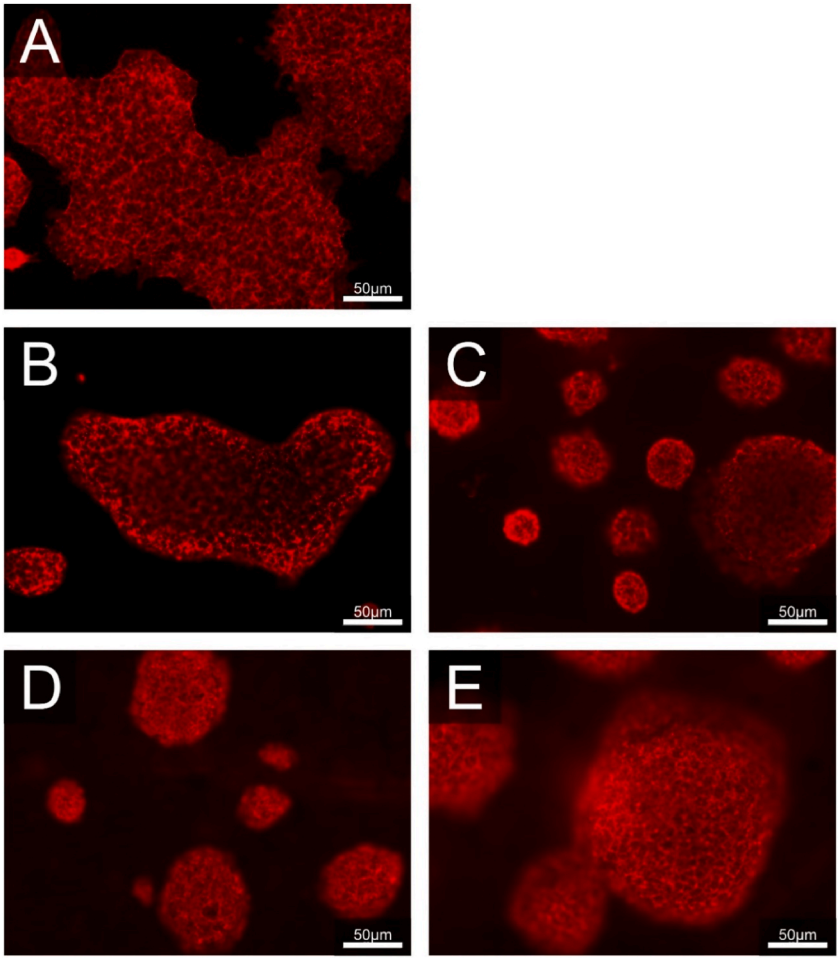

Fig. 9. Fluorescence microscopy images of R1 mouse embryonic stem cells cultivated on: (**A**) Reference; (**B**) isotropic PU mat with Alb/Gel; (**C**) anisotropic PU mat with Alb/Gel; (**D**) isotropic PUPPy composite with Alb/Gel; (**E**) anisotropic PUPPy composite with Alb/Gel. Reference cells were cultivated in cell culture dishes. Red color: ActinRed – actin. Magnification: 100 × . (For interpretation of the references to color in this figure legend, the reader is referred to the Web version of this article.)

different shapes and sizes were observed on each of them, regardless of the presence or absence of anisotropy or the PPy coating. In general, neither the fiber orientation nor the conductive PPy coating had a visible impact on the morphology of embryonic stem cells. The inert response of undifferentiated stem cells indicates that the coating can be applied without inducing unwanted differentiation or altering the basic properties of stem cells and suggests that the used coatings do not interfere with the fundamental stem cell characteristics, thus preserving their stemness.

4. Conclusions

This work presents a simple and fast *in situ* PPy coating technique applicable to different types of substrates. Here presented chemical synthesis of the coatings conducted at room temperature in an aqueous solution takes only a few seconds and does not require stabilizers or other modifiers. The findings demonstrate that the earlier the polymerization procedure is terminated, the more uniform PPy layer is produced. Furthermore, PPy coatings produced in 15 s retain good conductivity. Variations in PPy coatings were observed depending on the oxidizing agent utilized (APS vs $FeCl_3$). The coatings varied in conductivity, roughness, and thickness. On the other hand, both PPy^{APS} and PPy^{FeCl3} coatings showed limitations in their cytocompatibility, which was affected by their surface free energies. This limitation is however eliminated by techniques commonly used in cell cultures, coating with Alb/Gel.

Anisotropy, another factor influencing material/cell interactions, was introduced to PPy coating by its deposition on electrospun nonwoven nanofiber PU mats with manually uniaxially oriented fibers. The fiber alignment showed a significant effect on the morphology of mouse fibroblasts. Proven by cell image analyses, not only cytoskeletons but also cell nuclei demonstrated elongated shapes with uniform orientation strictly along the fibers. The PPy coating with Alb/Gel on the anisotropic PU mat suppresses fiber alignment's impact on fibroblast morphology while ensuring a uniform surface, crucial for tissue regeneration and wound healing

processes. Neither the coating nor fiber alignment visibly affects mouse embryonic stem cell behavior, preserving their fundamental properties without inducing unwanted differentiation.

The results of this study highlight the importance of the reaction time in the *in situ* synthesis of PPy coatings. Furthermore, it also deepens the current understanding of the impacts of polymer surface properties on cell behavior and hence contributes to the optimization of scaffold design with respect to achieving the growth of specific cells/tissues.

CRediT authorship contribution statement

Leona Mahelová: Writing – review & editing, Writing – original draft, Visualization, Software, Methodology, Investigation, Formal analysis, Data curation, Conceptualization. **Petr Slobodian:** Resources, Investigation. **Karolína Kocourková:** Investigation. **Antonín Minařík:** Investigation. **Robert Moučka:** Investigation. **Miroslava Trchová:** Investigation. **Martina Martínková:** Methodology. **Kateřina Skopalová:** Methodology. **Zdenka Víchová:** Methodology, Funding acquisition. **Věra Kašpárková:** Writing – review & editing, Validation, Supervision, Methodology. **Petr Humpolíček:** Writing – review & editing, Writing – original draft, Visualization, Validation, Supervision, Resources, Project administration, Methodology, Funding acquisition, Formal analysis, Data curation, Conceptualization.

Declaration of competing interest

The authors declare that they have no known competing financial interests or personal relationships that could have appeared to influence the work reported in this paper.

Acknowledgments

The authors acknowledge the support by the Czech Science Foundation (23-07425S). The project of Ministry of Education, Youth and Sports of the Czech Republic – DKRVO (RP/CPS/2022/001 and RP/CPS/2022/007) and Internal Grant Agency of Tomas Bata University in Zlín, Czech Republic (IGA/CPS/2024/007) are also acknowledged. The authors thank Ing. Daniela Minaříková, Ph.D. for her contribution to the preliminary study of polypyrrole thin films.

References

[1] M. Gajendiran, et al., Conductive biomaterials for tissue engineering applications, J. Ind. Eng. Chem. 51 (2017) 12–26, https://doi.org/10.1016/j.jiec.2017.02.031. Jul.
[2] G. Shi, M. Rouabhia, Z. Wang, L.H. Dao, Z. Zhang, A novel electrically conductive and biodegradable composite made of polypyrrole nanoparticles and polylactide, Biomaterials 25 (13) (2004) 2477–2488, https://doi.org/10.1016/j.biomaterials.2003.09.032. Jun.
[3] J. Huang, et al., Electrical stimulation to conductive scaffold promotes axonal regeneration and remyelination in a rat model of large nerve defect, PLoS One 7 (6) (2012) e39526, https://doi.org/10.1371/journal.pone.0039526. Jun.
[4] L. Mohammadi Amirabad, et al., Enhanced cardiac differentiation of human cardiovascular disease patient-specific induced pluripotent stem cells by applying unidirectional electrical pulses using aligned electroactive nanofibrous scaffolds, ACS Appl. Mater. Interfaces 9 (8) (2017) 6849–6864, https://doi.org/10.1021/acsami.6b15271. Mar.
[5] X. Wang, et al., Evaluation of biocompatibility of polypyrrole in vitro and in vivo, J. Biomed. Mater. Res. 68A (3) (2004) 411–422, https://doi.org/10.1002/jbm.a.20065.
[6] D. d Ateh, H. a Navsaria, P. Vadgama, Polypyrrole-based conducting polymers and interactions with biological tissues, J. R. Soc. Interface 3 (11) (2006) 741–752, https://doi.org/10.1098/rsif.2006.0141. Dec.
[7] P. Humpolicek, et al., The biocompatibility of polyaniline and polypyrrole: a comparative study of their cytotoxicity, embryotoxicity and impurity profile, Mater. Sci. Eng., C 91 (2018) 303–310, https://doi.org/10.1016/j.msec.2018.05.037. Oct.
[8] K. Skopalova, et al., Modulation of differentiation of embryonic stem cells by polypyrrole: the impact on neurogenesis, Int. J. Mol. Sci. 22 (2) (2021) 501, https://doi.org/10.3390/ijms22020501. Jan.
[9] N. Ferraz, M. Strømme, B. Fellström, S. Pradhan, L. Nyholm, A. Mihranyan, In vitro and in vivo toxicity of rinsed and aged nanocellulose–polypyrrole composites, J. Biomed. Mater. Res. 100A (8) (2012) 2128–2138, https://doi.org/10.1002/jbm.a.34070.
[10] S.P. Armes, Optimum reaction conditions for the polymerization of pyrrole by iron(III) chloride in aqueous solution, Synth. Met. 20 (3) (1987) 365–371, https://doi.org/10.1016/0379-6779(87)90833-2. Jun.
[11] J. Duchet, R. Legras, S. Demoustier-Champagne, Chemical synthesis of polypyrrole: structure–properties relationship, Synth. Met. 98 (2) (1998) 113–122, https://doi.org/10.1016/S0379-6779(98)00180-5. Dec.
[12] J. Upadhyay, A. Kumar, B. Gogoi, A.K. Buragohain, Biocompatibility and antioxidant activity of polypyrrole nanotubes, Synth. Met. 189 (2014) 119–125, https://doi.org/10.1016/j.synthmet.2014.01.004. Mar.
[13] P. Keša, et al., Photoacoustic properties of polypyrrole nanoparticles, Nanomaterials 11 (9) (2021), https://doi.org/10.3390/nano11092457. Art. no. 9, Sep.
[14] Ya O. Mezhuev, et al., Synthesis of aqueous polypyrrole dispersions stabilized with polyvinyl alcohol and preparation of hemocompatible films based on them, Russ. J. Appl. Chem. 88 (6) (2015) 1026–1032, https://doi.org/10.1134/S107042721506021X.
[15] A. Pich, Y. Lu, H.-J.P. Adler, Polymeric particles with conjugated polymer: layer on its surface as effective adsorbents of amino acids, Polymer 47 (19) (Sep. 2006) 6536–6543, https://doi.org/10.1016/j.polymer.2006.07.055.
[16] A. Vaitkuviene, et al., Some biocompatibility aspects of conducting polymer polypyrrole evaluated with bone marrow-derived stem cells, Colloids Surf. A Physicochem. Eng. Asp. 442 (2014) 152–156, https://doi.org/10.1016/j.colsurfa.2013.06.030. Feb.
[17] M. Sak-Bosnar, M.V. Budimir, S. Kovac, D. Kukulj, L. Duic, Chemical and electrochemical characterization of chemically synthesized conducting polypyrrole, J. Polym. Sci. Polym. Chem. 30 (8) (1992) 1609–1614, https://doi.org/10.1002/pola.1992.080300813.
[18] A. Razaq, A. Mihranyan, K. Welch, L. Nyholm, M. Strømme, Influence of the type of oxidant on anion exchange properties of fibrous cladophora cellulose/polypyrrole composites, J. Phys. Chem. B 113 (2) (2009) 426–433, https://doi.org/10.1021/jp806517h. Jan.
[19] X. Chen, J.-P. Issi, J. Devaux, D. Billaud, Chemically oxidized polypyrrole: influence of the experimental conditions on its electrical conductivity and morphology, Polym. Eng. Sci. 35 (8) (1995) 642–647, https://doi.org/10.1002/pen.760350803.
[20] A. Azioune, M.M. Chehimi, B. Miksa, T. Basinska, S. Slomkowski, Hydrophobic Protein−Polypyrrole interactions: the role of van der Waals and lewis Acid−Base forces as determined by contact angle measurements, Langmuir 18 (4) (2002) 1150–1156, https://doi.org/10.1021/la010444o. Feb.

[21] A. Azioune, K. Pech, B. Saoudi, M.M. Chehimi, G.P. McCarthy, S.P. Armes, Adsorption of human serum albumin onto polypyrrole powder and polypyrrole-silica nanocomposites, Synth. Met. 102 (1) (1999) 1419–1420, https://doi.org/10.1016/S0379-6779(98)00982-5. Jun.

[22] E.A. Sanches, et al., Nanostructured polypyrrole powder: a structural and morphological characterization, J. Nanomater. 2015 (2015) e129678, https://doi.org/10.1155/2015/129678. Sep.

[23] K.A. Noh, D.-W. Kim, C.-S. Jin, K.-H. Shin, J.H. Kim, J.M. Ko, Synthesis and pseudo-capacitance of chemically-prepared polypyrrole powder, J. Power Sources 124 (2) (2003) 593–595, https://doi.org/10.1016/S0378-7753(03)00813-9. Nov.

[24] B. Ustamehmetoğlu, N. Kizilcan, A.S. Saraç, A. Akar, Soluble polypyrrole copolymers, J. Appl. Polym. Sci. 82 (5) (2001) 1098–1106, https://doi.org/10.1002/app.1944.

[25] C. Biran, L. Toppare, T. Tinçer, Y. Yağci, V. Harabagiu, Mechanical properties of conducting H-type polysiloxane–polypyrrole graft copolymers and polytetrahydrofuran–polypyrrole block copolymers, J. Appl. Polym. Sci. 86 (7) (2002) 1663–1666, https://doi.org/10.1002/app.11031.

[26] O. Gunaydin, L. Toppare, Y. Yagci, V. Harabagiu, M. Pintela, B.C. Simionescu, Synthesis of conducting polysiloxane — polypyrrole graft copolymers, Polym. Bull. 47 (6) (2002) 501–508, https://doi.org/10.1007/s002890200014. Feb.

[27] M. Omastová, et al., Towards conducting inks: polypyrrole–silver colloids, Electrochim. Acta 122 (2014) 296–302, https://doi.org/10.1016/j.electacta.2013.11.037. Mar.

[28] A. Zelenev, W. Sonnenberg, E. Matijević, Preparation, characterization, and adhesion of monodispersed polypyrrole particles, Colloid Polym. Sci. 276 (9) (1998) 838–841, https://doi.org/10.1007/s003960050318. Oct.

[29] S. Káčerová, et al., Biocompatibility of colloidal polypyrrole, Colloids Surf. B Biointerfaces 232 (2023) 113605, https://doi.org/10.1016/j.colsurfb.2023.113605. Dec.

[30] S. Maity, Optimization of processing parameters of in-situ polymerization of pyrrole on woollen textile to improve its thermal conductivity, Prog. Org. Coating 107 (2017) 48–53, https://doi.org/10.1016/j.porgcoat.2017.03.010. Jun.

[31] Q. Zhu, et al., Epoxy coating with in-situ synthesis of polypyrrole functionalized graphene oxide for enhanced anticorrosive performance, Prog. Org. Coating 140 (2020) 105488, https://doi.org/10.1016/j.porgcoat.2019.105488. Mar.

[32] Y. Zhao, et al., A novel flexible sensor for respiratory monitoring based on in situ polymerization of polypyrrole and polyurethane coating, RSC Adv. 7 (78) (2017) 49576–49585, https://doi.org/10.1039/C7RA08331A. Oct.

[33] N. Maráková, et al., Antimicrobial activity and cytotoxicity of cotton fabric coated with conducting polymers, polyaniline or polypyrrole, and with deposited silver nanoparticles, Appl. Surf. Sci. 396 (2017) 169–176, https://doi.org/10.1016/j.apsusc.2016.11.024. Feb.

[34] R. Ravichandran, S. Sundarrajan, J.R. Venugopal, S. Mukherjee, S. Ramakrishna, Applications of conducting polymers and their issues in biomedical engineering, J. R. Soc. Interface 7 (suppl_5) (2010), https://doi.org/10.1098/rsif.2010.0120.focus. Oct.

[35] B. Garner, A.J. Hodgson, G.G. Wallace, P.A. Underwood, Human endothelial cell attachment to and growth on polypyrrole-heparin is vitronectin dependent, J. Mater. Sci. Mater. Med. 10 (1) (1999) 19–27, https://doi.org/10.1023/A:1008835925998. Jan.

[36] P. Slepička, N. Slepičková Kasálková, L. Bačáková, Z. Kolská, V. Švorčík, Enhancement of polymer cytocompatibility by nanostructuring of polymer surface, J. Nanomater. 2012 (2012) e527403, https://doi.org/10.1155/2012/527403. Jul.

[37] C.J. Wilson, R.E. Clegg, D.I. Leavesley, M.J. Pearcy, Mediation of biomaterial–cell interactions by adsorbed proteins: a review, Tissue Eng. 11 (1–2) (2005) 1–18, https://doi.org/10.1089/ten.2005.11.1. Jan.

[38] G.R. Mitchell, A. Tojeira, Role of anisotropy in tissue engineering, Procedia Eng. 59 (2013) 117–125, https://doi.org/10.1016/j.proeng.2013.05.100.

[39] M.E. Hoque, Robust formulation for the design of tissue engineering scaffolds: a comprehensive study on structural anisotropy, viscoelasticity and degradation of 3D scaffolds fabricated with customized desktop robot based rapid prototyping (DRBRP) system, Mater. Sci. Eng. C 72 (Mar. 2017) 433–443, https://doi.org/10.1016/j.msec.2016.11.019.

[40] N. Bursac, K.K. Parker, S. Iravanian, L. Tung, Cardiomyocyte cultures with controlled macroscopic anisotropy, Circ. Res. 91 (12) (2002) e45–e54, https://doi.org/10.1161/01.RES.0000047530.88338.EB. Dec.

[41] M. Nikkhah, F. Edalat, S. Manoucheri, A. Khademhosseini, Engineering microscale topographies to control the cell–substrate interface, Biomaterials 33 (21) (2012) 5230–5246, https://doi.org/10.1016/j.biomaterials.2012.03.079. Jul.

[42] F. Yang, R. Murugan, S. Wang, S. Ramakrishna, Electrospinning of nano/micro scale poly(l-lactic acid) aligned fibers and their potential in neural tissue engineering, Biomaterials 26 (15) (2005) 2603–2610, https://doi.org/10.1016/j.biomaterials.2004.06.051. May.

[43] Z. Yin, et al., The regulation of tendon stem cell differentiation by the alignment of nanofibers, Biomaterials 31 (8) (2010) 2163–2175, https://doi.org/10.1016/j.biomaterials.2009.11.083. Mar.

[44] P. Humpolicek, et al., Polyaniline cryogels: biocompatibility of novel conducting macroporous material, Sci. Rep. 8 (2018) 135, https://doi.org/10.1038/s41598-017-18290-1. Jan.

[45] K.A. Milakin, et al., Biocompatible and antibacterial gelatin-based polypyrrole cryogels, Polymer 197 (2020) 122491, https://doi.org/10.1016/j.polymer.2020.122491. May.

[46] F. Golgovici, M.-S. Cărlan, A.-G. Popescu, L. Anicai, Electrochemical synthesis of polypyrrole and polypyrrole-indomethacin coatings on NiCr alloys involving deep eutectic solvents, Metals 10 (9) (2020), https://doi.org/10.3390/met10091130. Art. no. 9, Sep.

[47] J. Thunberg, et al., In situ synthesis of conductive polypyrrole on electrospun cellulose nanofibers: scaffold for neural tissue engineering, Cellulose 22 (3) (2015) 1459–1467, https://doi.org/10.1007/s10570-015-0591-5. Jun.

[48] A. Wu, H. Kolla, S.K. Manohar, Chemical synthesis of highly conducting polypyrrole nanofiber film, Macromolecules 38 (19) (2005) 7873–7875, https://doi.org/10.1021/ma051299e. Sep.

[49] S. Sahoo, G. Karthikeyan, G. Ch Nayak, C.K. Das, Electrochemical characterization of in situ polypyrrole coated graphene nanocomposites, Synth. Met. 161 (15) (2011) 1713–1719, https://doi.org/10.1016/j.synthmet.2011.06.011. Aug.

[50] N. Vellguth, M. Shamsuyeva, S. Kroll, F. Renz, H.-J. Endres, Electrical conductivity in biocomposites via polypyrrole coating, J. Mater. Sci. Mater. Electron. 30 (3) (2019) 2373–2381, https://doi.org/10.1007/s10854-018-0510-2. Feb.

[51] A. Nagy, J. Rossant, R. Nagy, W. Abramow-Newerly, J.C. Roder, Derivation of completely cell culture-derived mice from early-passage embryonic stem cells, Proc. Natl. Acad. Sci. USA 90 (18) (1993) 8424–8428, https://doi.org/10.1073/pnas.90.18.8424. Sep.

[52] A.E. Carpenter, et al., CellProfiler: image analysis software for identifying and quantifying cell phenotypes, Genome Biol. 7 (10) (2006) R100, https://doi.org/10.1186/gb-2006-7-10-r100.

[53] A.L. Pang, A. Arsad, M. Ahmadipour, Synthesis and factor affecting on the conductivity of polypyrrole: a short review, Polym. Adv. Technol. 32 (4) (2021) 1428–1454, https://doi.org/10.1002/pat.5201. Apr.

[54] N.K. Guimard, N. Gomez, C.E. Schmidt, Conducting polymers in biomedical engineering, Prog. Polym. Sci. 32 (8) (2007) 876–921, https://doi.org/10.1016/j.progpolymsci.2007.05.012. Aug.

[55] T. Patois, B. Lakard, N. Martin, P. Fievet, Effect of various parameters on the conductivity of free standing electrosynthesized polypyrrole films, Synth. Met. 160 (19) (2010) 2180–2185, https://doi.org/10.1016/j.synthmet.2010.08.005. Oct.

[56] V. Kašpárková, et al., Cell-compatible conducting polyaniline films prepared in colloidal dispersion mode, Colloids Surf. B Biointerfaces 157 (2017) 309–316, https://doi.org/10.1016/j.colsurfb.2017.05.066. Sep.

[57] M. Mahmoodian, B. Pourabbas, S. Mohajerzadeh, Effect of anionic dopants on thickness, morphology and electrical properties of polypyrrole ultra-thin films prepared by in situ chemical polymerization, Thin Solid Films 583 (2015) 255–263, https://doi.org/10.1016/j.tsf.2015.03.043. May.

[58] C. Sasso, D. Beneventi, E. Zeno, D. Chaussy, M. Petit-Conil, N. Belgacem, Polypyrrole and polypyrrole/wood-derived materials conducting composites: a review, Bioresources 6 (3) (2011) 3585–3620.

[59] S.T. Navale, A.T. Mane, A.A. Ghanwat, A.R. Mulik, V.B. Patil, Camphor sulfonic acid (CSA) doped polypyrrole (PPy) films: measurement of microstructural and optoelectronic properties, Measurement 50 (2014) 363–369, https://doi.org/10.1016/j.measurement.2014.01.012. Apr.

[60] J. Berg, L. Eriksson, P. Claesson, K. Borve, 3-Component Langmuir-Blodgett-Films with a controllable degree of polarity, Langmuir 10 (4) (1994) 1225–1234, https://doi.org/10.1021/la00016a041. Apr.
[61] E.A. Vogler, Structure and reactivity of water at biomaterial surfaces, Adv. Colloid Interface Sci. 74 (1) (1998) 69–117, https://doi.org/10.1016/S0001-8686(97)00040-7. Feb.
[62] J. Stejskal, M. Trchová, Conducting polypyrrole nanotubes: a review, Chem. Pap. 72 (7) (2018) 1563–1595, https://doi.org/10.1007/s11696-018-0394-x. Jul.
[63] M.R. Abidian, J.M. Corey, D.R. Kipke, D.C. Martin, Conducting-polymer nanotubes improve electrical properties, mechanical adhesion, neural attachment, and neurite outgrowth of neural electrodes, Small 6 (3) (2010) 421–429, https://doi.org/10.1002/smll.200901868.
[64] C. Satriano, S. Carnazza, S. Guglielmino, G. Marletta, Surface free energy and cell attachment onto ion-beam irradiated polymer surfaces, Nucl. Instrum. Methods Phys. Res. Sect. B Beam Interact. Mater. Atoms 208 (2003) 287–293, https://doi.org/10.1016/S0168-583X(03)00647-5. Aug.
[65] M. Tallawi, et al., Strategies for the chemical and biological functionalization of scaffolds for cardiac tissue engineering: a review, J. R. Soc. Interface 12 (108) (2015) 20150254, https://doi.org/10.1098/rsif.2015.0254. Jul.
[66] M. Wu, C. Zhong, Y. Deng, Q. Zhang, X. Zhang, X. Zhao, Resveratrol loaded glycyrrhizic acid-conjugated human serum albumin nanoparticles for tail vein injection II: pharmacokinetics, tissue distribution and bioavailability, Drug Deliv. 27 (1) (Jan. 2020) 81–90, https://doi.org/10.1080/10717544.2019.1704944.
[67] S. Van Vlierberghe, E. Vanderleyden, V. Boterberg, P. Dubruel, Gelatin functionalization of biomaterial surfaces: strategies for immobilization and visualization, Polymers 3 (1) (2011), https://doi.org/10.3390/polym3010114. Art. no. 1, Mar.
[68] T. Fee, C. Downs, A. Eberhardt, Y. Zhou, J. Berry, Image-based quantification of fiber alignment within electrospun tissue engineering scaffolds is related to mechanical anisotropy, J. Biomed. Mater. Res. 104 (7) (2016) 1680–1686, https://doi.org/10.1002/jbm.a.35697.
[69] C.-H. Lin, X. Tang, P. Chen, S.-C. Luo, Unraveling the adhesion behavior of different cell lines on biomimetic PEDOT interfaces: the role of surface morphology and antifouling properties, ACS Appl. Bio Mater. (2023), https://doi.org/10.1021/acsabm.3c00833. Nov.
[70] C.M. Tringides, D.J. Mooney, Conductive hydrogel scaffolds for the 3D localization and orientation of fibroblasts, Macromol. Biosci. 24 (1) (2024) 2300044, https://doi.org/10.1002/mabi.202300044.